Journal of Solid State Chemistry 187 (2012) 27–34

Contents lists available at SciVerse ScienceDirect

Journal of Solid State Chemistry

journal homepage: www.elsevier.com/locate/jssc

Neutron diffraction study of the monoclinic to tetragonal structural transition in $LaNbO_4$ and its relation to proton mobility

M. Huse [a], A.W.B. Skilbred [a], M. Karlsson [b], S.G. Eriksson [c], T. Norby [a], R. Haugsrud [a], C.S. Knee [d,*]

[a] Department of Chemistry, University of Oslo, FERMiO, Gaustadalléen 21, NO-0349 Oslo, Norway
[b] Department of Applied Physics, Chalmers University of Technology, SE-412 96 Gothenburg, Sweden
[c] Department of Environmental Inorganic Chemistry, Chalmers University of Technology, SE-412 96 Gothenburg, Sweden
[d] Department of Chemistry, University of Gothenburg, SE-412 96 Gothenburg, Sweden

ARTICLE INFO

Article history:
Received 11 October 2011
Received in revised form
14 December 2011
Accepted 18 December 2011
Available online 26 December 2011

Keywords:
Proton conductors
Neutron diffraction
Structural phase transition
Fuel cell electrolytes

ABSTRACT

The fergusonite-scheelite structural transition of $LaNbO_4$ was characterized by high-intensity variable temperature neutron powder diffraction in an effort to link structural changes to proton transport in the low temperature monoclinic and high temperature tetragonal polymorphs. The pronounced decrease in enthalpy of proton mobility with increasing temperature in monoclinic $LaNbO_4$, identified by Fjeld et al. [1], was found to coincide with the decrease in a key inter-tetrahedral oxygen separation. At temperatures above the transition, this oxygen to oxygen distance remains constant, behavior that is consistent with the invariant nature of the calculated enthalpy of mobility for the tetragonal phase. This oxygen separation is therefore proposed as the key structural parameter determining the success rate of proton transfer and ultimately the proton diffusion in $LaNbO_4$. Infrared measurements performed on acceptor-doped $LaNbO_4$ show an absorption in the region 2500 to 3700 cm^{-1} attributed to the O–H stretching motion influenced by hydrogen bonding.

1. Introduction

The ABO_4-type family (silicates, germanates, molybdates, tungstates, niobates, tantalates, vanadates, phosphates etc.) is a class of materials with several proposed areas of application, e.g. laser-host materials, gas separation membranes, fuel cell electrolytes [2,3]. The class exhibits several structural phase transitions as a function of temperature and pressure in the sequence from orthorhombic via monoclinic to tetragonal symmetry [4,5]. $LaNbO_4$ is one member of this family exhibiting a phase transition between monoclinic and tetragonal symmetry. Structural studies of $LaNbO_4$ may be dated back as early as in the 1950's [6], however renewed interest has emerged in the last decade due to the discovery of appreciable proton conductivity ($\sigma_{H^+} \approx 10^{-3}$ S cm^{-1} at 900 °C) and a proton transference number of approximately unity [3,7]. Recently, it has been shown by thermogravimetry that $LaNbO_4$ is stable in CO_2 and CO_2+H_2O atmospheres [8]. Consequently, this material is an interesting candidate material for the electrolyte in fuel cells or hydrogen sensors operating in CO_2-rich and other acidic atmospheres.

In comparison to the widely studied cubic or orthorhombic proton conducting perovskites, the crystal structure of $LaNbO_4$ is considerably more anisotropic in nature. Furthermore, in contrast to the perovskites, acceptor-doped $LaNbO_4$ displays a high temperature phase transition that clearly influences the proton conductivity [3,7]. The phase transformation of $LaNbO_4$ from monoclinic (m-$LaNbO_4$) to tetragonal (t-$LaNbO_4$) symmetry with increasing temperature has received considerable attention in the literature. It has been characterized by Jian and Wayman [5] as a second order phase transition between the ferroelastic monoclinic phase and the paraelastic tetragonal phase. Both structures contain isolated NbO_4-tetrahedra interlinked with La-ions of eight-fold coordination to oxygen [5,9]. The transition temperature, $T_{trans.}$, is reported in the range 510 ± 15 °C [5,7,10–12].

The low temperature phase has been assigned to the monoclinic structure (space group, SG $I2/a$, No. 15, $Z=4$) which is isostructural to the mineral fergusonite ($YNbO_4$) [4,5]. The unit cell of m-$LaNbO_4$ has cell parameters of $a=5.567$ Å, $b=5.204$ Å and $c=11.53$ Å with a $\beta=94.1$ °C, leaving a unit cell volume of 333.18 $Å^3$ [13], which is displayed in Fig. 1a. Nb has a coordination of 4 to oxygen, forming isolated distorted tetrahedral units. There are two oxygen positions in the low temperature phase, at a distance with respect to the Nb of approx. 1.90 Å and 1.85 Å, at room temperature for O(1) and O(2), respectively. La has only one position in the structure; however the La has an alternating inter-layer distance in the b-direction, where the layer of O(1)-ions gives a shorter distance and the layer of O(2)-ions the longer inter-layer distance. The high temperature phase has a tetragonal

* Corresponding author.
E-mail address: knee@chem.gu.se (C.S. Knee).

0022-4596/$ - see front matter © 2012 Elsevier Inc. All rights reserved.
doi:10.1016/j.jssc.2011.12.025

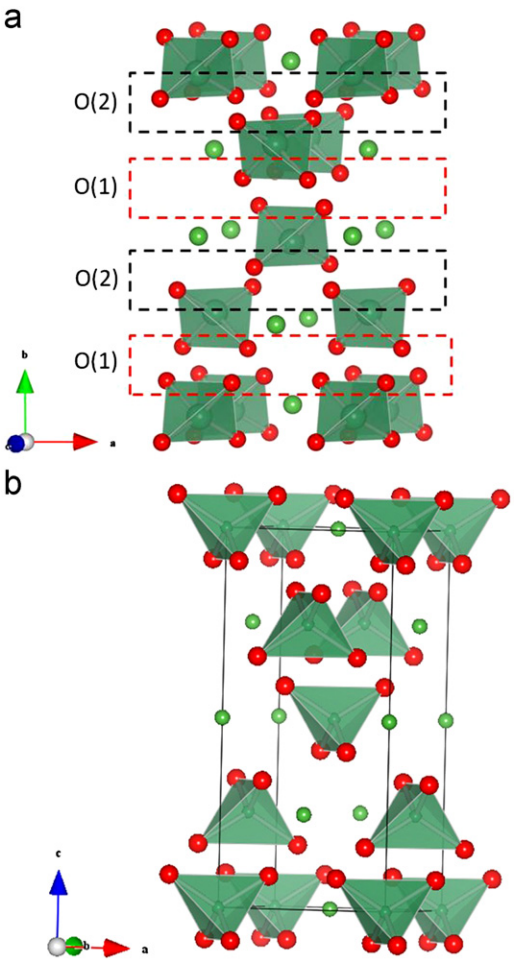

Fig. 1. (a) Structure of monoclinic $LaNbO_4$ where *b*-direction represents the long axis of the monoclinic structure. Atomic positions from Tsunekawa et al. [18] and illustrative inspiration from Fjeld et al. [1]. Tetrahedral NbO_4 units are shown. Dashed lines represent the two different layers of oxygen sites O(1) (red line) and O(2) (black line). (b) Structure of tetragonal $LaNbO_4$ where the *c*-direction represents the long axis. Atomic positions from David [4]. Oxygen (red spheres), lanthanum (green spheres) and niobium (inside tetrahedra). (For interpretation of the references to color in this figure legend, the reader is referred to the web version of this article.)

structure (SG $I4_1/a$ No. 88, $Z=4$) shown in Fig. 1*b*, which is isostructural to the structure of scheelite, $CaWO_4$. In *t*-$LaNbO_4$, oxygen has one site and the La-layers have equal inter-atomic distances.

Haugsrud and co-workers [3,7,10] have extensively studied the conductivity behavior of $LaNbO_4$, both nominally undoped and doped (Sr, Ca, Ba etc.), in various atmospheres and in a temperature range from 300 to 1200 °C. When the conductivity of acceptor doped $LaNbO_4$ in wet atmosphere is plotted vs. inverse absolute temperature, a bend in the conductivity curve at the onset of the phase transition may be observed [7]. This is traditionally interpreted as an abrupt change in the enthalpy of proton mobility at this temperature. However, a more recent study [1] suggests a different interpretation, where the bend in the conductivity data is explained by a gradual increase in the enthalpy of proton mobility with decreasing temperature and decreasing symmetry in the monoclinic phase. This more rigorous analysis of conductivity data through a second order phase transition indicates that the enthalpy of proton mobility increases from 35 kJ/mol at T_{trans} to 57 kJ/mol at 205 °C [1]. The enthalpy of proton mobility in the high temperature tetragonal phase was reported experimentally to be 35 kJ/mol and computationally 39 kJ/mol and to be constant with temperature [1]. The values of the enthalpy of proton mobility in the literature show some variation due to different interpretations and whether mobilities are deduced from experimental measurements or calculations [1,7].

In the same study Fjeld et al. employed density functional theory (DFT) to investigate possible stable proton sites for both polymorphs of $LaNbO_4$. The main findings are that in the low *T* monoclinic phase (referred to from here on as *m*-$LaNbO_4$) the protons strongly favor sites bonding to the O(1) oxygen, and that for long range diffusion hopping of the protons between NbO_4 tetrahedra separated along the *b*-axis is rate limiting. Another recent computational study of $LaNbO_4$ probed dopant ion solubility, oxygen vacancy formation and protonic sites [14].

In the present study we have performed a variable temperature (VT) structural study of $LaNbO_4$ using neutron diffraction. Our overall aim was to better characterize the monoclinic to tetragonal structural transition in order to explain the differing mobility of protons in the high and low temperature structures.

2. Experimental

$LaNbO_4$ was synthesized following the solid state route with La_2O_3 (99.99%, Alfa Aesar) and Nb_2O_5 (99.9%, Alfa Aesar) as starting powders. Due to the hygroscopic nature of La_2O_3, this powder was heat-treated at 900 °C for 3 h followed by rapid cooling to room temperature under a drying agent, prior to weighing to ensure dehydration of lanthanum hydroxide to lanthanum oxide (La_2O_3) [15]. Stoichiometric amounts of the powders were thereafter mixed in isopropanol in an agate mortar for 20 min, calcined at 950 °C for 15 h in air, and finally remixed in a mortar before being pressed into a pellet for a second calcination at 1000 °C for 15 h.

Room temperature powder X-ray diffraction (XRD, D5000, Siemens) was performed with Cu $K_{\alpha 1}$ radiation. In order to determine estimates of the cell parameters and confirm phase purity, Le Bail fitting of the X-ray pattern was performed using the software, FullProf [16]. Neutron powder diffraction (NPD) data were collected on manually ground powder samples using the D20 high-flux neutron diffractometer at the Institut Laue-Langevin in Grenoble, France, operating with an incident neutron wavelength of 1.48 Å in high-resolution mode [17]. The $LaNbO_4$ sample was placed in a silica tube open to the air and heated using the standard D20 furnace. To correct for the background, data from an empty silica tube inside the furnace was subtracted. Initially a RT scan was collected (5 min acquisition time) and then data were collected ($\sim$1 data set min^{-1}) on heating from RT to approximately 900 °C with a ramp rate of 1.0 °C/min. Analysis of the ramping data was performed using the SeqGSAS subroutine of the GSAS Rietveld refinement program [18], with 31 and 25 variables included for the monoclinic ($I2/a$) and tetragonal ($I4_1/a$) refinements, respectively. Additional longer data sets (20 min acquisition time) were collected during cooling at selected temperatures with 20 min allowed for equilibration prior to data collection at each temperature. Finally, a joint Rietveld analysis of the RT XRD and Neutron data was performed.

Measurements of the thermal expansion coefficient (TEC) of the ceramic sample were carried out with a dilatometer (DIL 402C, Netzsch Gmbh) in wet argon from room temperature to 1000 °C and back down with ramp rates of 2 °C/min. No significant hysteresis or sintering was observed. The initial sample length, L_0, was 28 mm.

Infrared spectra were measured over the region 2200–4500 cm^{-1} with a Bruker Alpha spectrometer equipped with the DRIFT diffuse reflectance module, a KBr beam splitter and a DTGS detector. The samples were $La_{0.995}Sr_{0.005}NbO_{4-\delta}$ either hydrated under a flow of water saturated N_2 at 300 °C for 20 h, or dried under vacuum at 900 °C. The measurements were performed in an Ar glove box and the spectra were collected at room temperature. A measurement of

an Au standard was used as reference spectrum and the absorbance like spectra were derived by taking the logarithm between the reference spectra and the corresponding sample spectra. The absorbance like spectra were corrected by excluding minor impurity peaks at ~2350 and ~2950 cm^{-1}, attributable to asymmetric stretches of O–C–O and C–H stretches, respectively, and by subtracting a linearly sloping background in the range 2200–4500 cm^{-1}.

3. Results and discussion

3.1. Crystal structure at RT

Fig. 2 shows the Rietveld fit to the NPD RT data of $LaNbO_4$, and all diffraction peaks could be modeled satisfactorily using a monoclinic structure with the initial model taken from Tsunekawa et al. [19]. The cell parameters determined from the RT XRD and NPD data are in good agreement with each other and with literature values, as listed in Table 1, and it was possible to perform a successful joint analysis of the two data sets to yield the structural parameters listed in Table 2.

3.2. Crystal structure as a function of temperature

Inspection of the longer scan (20 min collection time) neutron diffraction measurements collected on cooling reveals a gradual peak splitting of the peaks at 2θ~27 ° and at ~44 ° into two more distinct peaks when going down in temperature from 560 °C to 280 °C as shown in Fig. 3. This is a typical feature of a material transforming from high to low symmetry and agrees well with the expected phase transition from tetragonal to monoclinic structure for $LaNbO_4$.

A feature of the analysis of the rapid ramping neutron data was the appearance of the tetragonal phase at temperatures significantly below the expected transition temperature. For

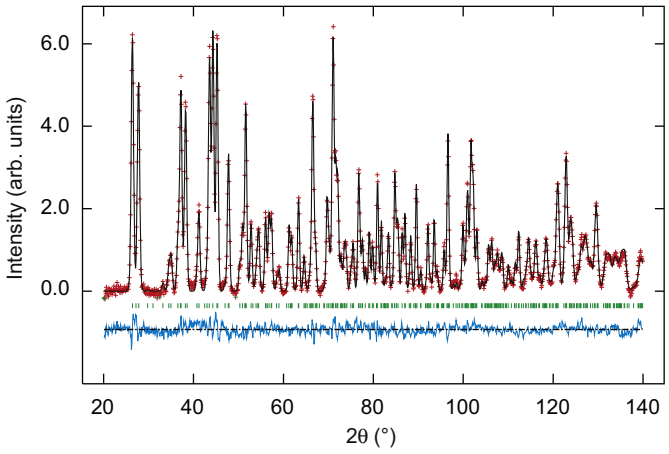

Fig. 2. Intensity vs. 2θ of NPD data of $LaNbO_4$ recorded in ambient air at RT. Crosses represent measured intensity and vertical ticks mark Bragg peaks according to the *I*2/*a* space group. The top line represents the profile calculated from Rietveld analysis and the bottom line is the difference between the observed and calculated patterns.

Table 2
Refined atomic coordinates and cell parameters from a joint Rietveld analysis of neutron (1299 data points) and PXRD (4486 data points) $LaNbO_4$ patterns collected at RT. Space group (*I*2/*a*).

Atom	*x*	*y*	*z*	U_{iso} (Å^2 × 100)
La	0.75	0.1230(2)	0.500000	1.37(4)
Nb	0.25	0.1037(2)	0.000000	1.14(6)
O(1)	0.4876(5)	0.2043(2)	0.1464(4)	0.97(5)
O(2)	0.0544(4)	0.0337(2)	0.2383(4)	1.05(5)
	a **(Å)**	***b*** **(Å)**	***c*** **(Å)**	***β*** **(°)**
	5.19954(8)	11.5196(2)	5.56168(8)	94.050(3)
χ^2	R_{wp} (%)	R_p (%)	Total No. of observables	No. of variables
1.88	5.31	4.22	5785	54

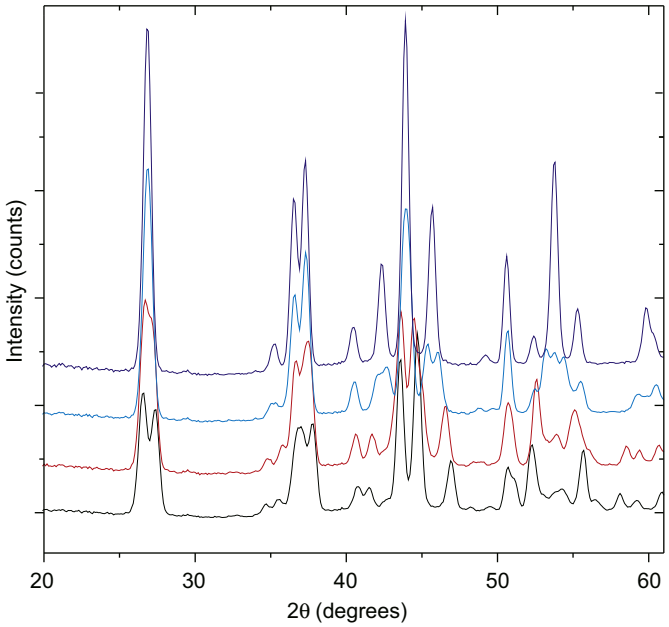

Fig. 3. Neutron powder diffraction patterns of $LaNbO_4$ at temperatures of 560 (top), 480, 400 and 280 °C (bottom).

Table 1
Cell parameters of $LaNbO_4$ from PXRD, and neutron powder diffraction for the low *T* and high *T* polymorphs, compared with literature data from Tsunekawa et al. [19] and David [4].

Diff. technique T	X-ray RT	Neutron RT	Neutron RT	Neutron 800 °C	Neutron 530 °C
Monoclinic				Tetragonal	
a **(Å)**	5.2021(9)	5.1997(2)	5.2015(1)	5.4069(2)	5.4001(2)
b **(Å)**	11.5208(19)	11.5181(4)	11.5194(2)	11.7011(5)	11.6661(2)
c **(Å)**	5.5617(10)	5.5612(2)	5.5647(1)	5.4069(2)	5.4001(2)
β **(°)**	94.046(7)	94.06(3)	94.100(1)	90	90
Vol (Å^3)	332.52(14)	332.22(19)	332.57(1)	342.07(2)	340.2
χ2	4.86	1.58	–	1.53	–
R_{wp} **(%)**	6.64	4.90	4.45	4.84	–
R_p **(%)**	4.94	4.00	3.42	3.94	–
Ref.	this study	this study	Tsunekawa [19]	this study	David [4]

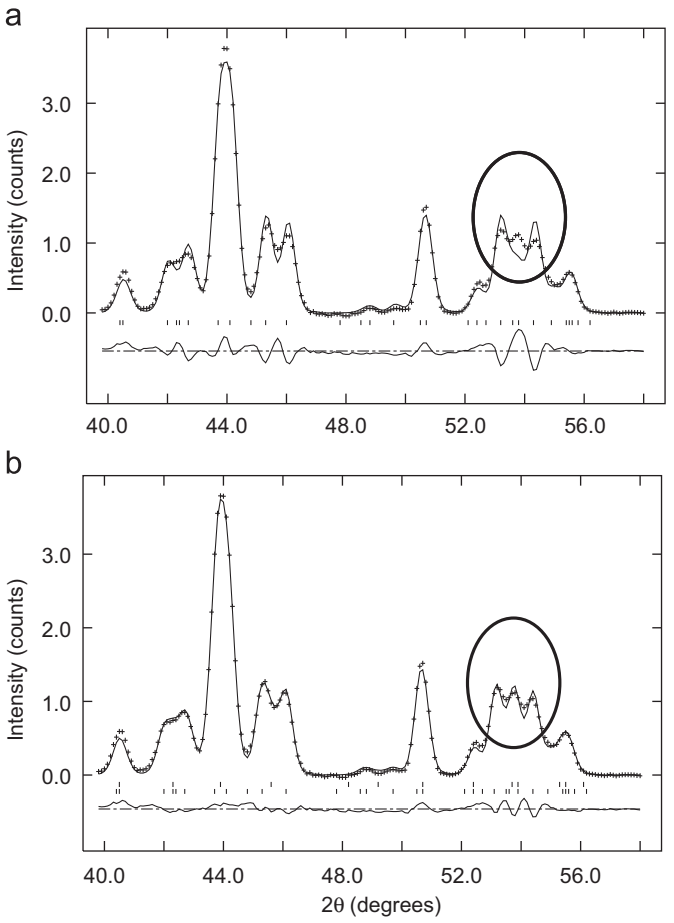

Fig. 4. Comparison of fits obtained to NPD data collected at $T=430$ °C whilst ramping with (a) monoclinic structural model only and (b) monoclinic (reflections marked by lower tick marks) and tetragonal (upper tick marks) structural models.

example, the introduction of a minority tetragonal phase (refined wt. % ≈ 20%) is required to satisfactorily model the data at $T=430$ °C, as illustrated in Fig. 4. The improvement in fit quality obtained using a two-phase approach is also reflected in the R_{wp} factor (R weighted profile) that falls from 5.92% to 4.26%. The observation of a two-phase region for $LaNbO_4$ is not expected as previous studies of the phase transition have assigned it as a continuous, second order, transition [4,5,20] and the coexistence of the two polymorphs at the same temperature thus violates Gibb's phase rule.

One possible explanation for the two phase behavior is the presence of a temperature gradient across the sample's ~3 cm height during the neutron measurements. In such a case at temperatures well below the transition the sample would be expected to have a distribution in the monoclinic lattice constants reflecting the spread of temperatures experienced by the sample. At temperatures where the temperature gradient covers the phase transition temperature, the sample would exhibit some domains with Bragg reflections representing the monoclinic polymorph and some the tetragonal polymorph. At higher temperatures, where the temperature gradient does not cover temperatures representing the monoclinic symmetry, the ND pattern will still reflect a distribution of cell parameters; the distribution will however be narrower due to the less pronounced temperature dependence of the cell parameters in the tetragonal polymorph. This interpretation is in good agreement with the observed NPD data. The fast heating rate employed may also contribute to the lack of thermal equilibration throughout the sample.

It should, however, be noted that a previous neutron diffraction study of $La_{0.99}Ca_{0.01}NbO_4$ by Malavasi et al. [21] also reported patterns where the introduction of a tetragonal model at temperatures significantly below the expected transition temperature improved the overall fit. These data were collected in much coarser temperature steps of 150 °C and with one hour equilibration dwells. Assuming that these previous results, and our current observations, were not affected by a temperature gradient across the sample, one may speculate whether more intrinsic factors are at play. Malavasi et al. suggested phase separation as a possible explanation. Alternatively, it is possible that the anomalous behavior is linked to the ferroelastic nature of the transition [4,12]. The transition temperature of individual domains may then be influenced by residual strain fields in the crystallites arising from the pelletisation step during synthesis. We note, however, that the majority of previous powder XRD studies of the $LaNbO_4$ phase transformation have not reported such a two-phase region [22,23]. We are therefore of the opinion that the presence of Bragg peaks from both polymorphs at temperatures in the vicinity of the transition temperature may be explained as a result of a thermal gradient. We stress that the refined structural parameters determined from the Rietveld analyses reflect the dominant phase at a given temperature; these derived structural parameters all show a smooth thermal dependence and are in good agreement with reported values from previous XRD and ND measurements of $LaNbO_4$.

As this is a study primarily motivated by rationalizing the different enthalpy of proton mobility in the two polymorphs of $LaNbO_4$, we continue with a focus on the evolving structural parameters extracted from the neutron data. We will start with the analysis of the cell parameters, before considering the Nb–O environment, and in particular the oxygen to oxygen separations critical for proton migration. Fig. 5 shows the thermal dependence of the cell constants of $LaNbO_4$ and cell volume, refined from neutron diffraction data fitted using a monoclinic (low T) and a tetragonal (high T) model. The figures are presented with some overlap, reflecting the ability to model the data near the transition with either phase.

The initial rapid changes seen in all the parameters reflect the fact that a linear heating rate is first established at $T \geq 100$ °C. From (Fig. 5a) it is clear that the monoclinic lattice parameters a and c converge to a common value ($a \approx 5.40$ Å) as the transition temperature is approached. Above the transition, thermal expansion in this plane is low. For $T > 100$ °C, the large cell parameter shows a fairly linear dependence up to the transition, above which the rate of expansion clearly reduces (inset Fig. 5b). The monoclinic angle, β, is ~94.1 °C at RT and it approaches 90 °C as the transition approaches (cf. Fig. 5c). It is evident from the behavior of the cell parameters, and cell volume (cf. Fig. 5b) that the thermal expansion is greatest in the monoclinic phase and that this behavior reflects primarily the differing rates of elongation of the long cell constant (b-parameter for m-$LaNbO_4$ / c-parameter for t-$LaNbO_4$) in both polymorphs.

Analysis of the cell volume data yielded linear thermal expansion coefficients (TEC) of $17.1 \cdot 10^{-6}\,K^{-1}$ and $4.2 \cdot 10^{-6}\,K^{-1}$ for the monoclinic and tetragonal phases, respectively. This compares to values of $15.3 \cdot 10^{-6}\,K^{-1}$ and $8.8 \cdot 10^{-6}\,K^{-1}$ obtained from dilatometry measurements on the same batch of sample (see Fig. 6), and reported values of $17.3 \cdot 10^{-6}\,K^{-1}$ and $7.1 \cdot 10^{-6}\,K^{-1}$ derived from a VT-PXRD analysis [22]. In the dilatometry data a change in the slope may be observed at $T \approx 500$ °C, reflecting the phase transition. The TECs for m-$LaNbO_4$ show reasonable agreement, but the TEC for the t-$LaNbO_4$ phase is significantly lower than that determined by dilatometry. Dilatometric measurements of polycrystalline materials results in linear thermal expansion coefficients, reflecting an average expansion of all the crystallographic directions of the material with temperature. The discrepancy between the TECs of the high T phase may be linked to the highly anisotropic expansion with temperature of $LaNbO_4$ and the fact that dilatometry measures the macroscopic elongation in one direction only compared to ND measurements which are

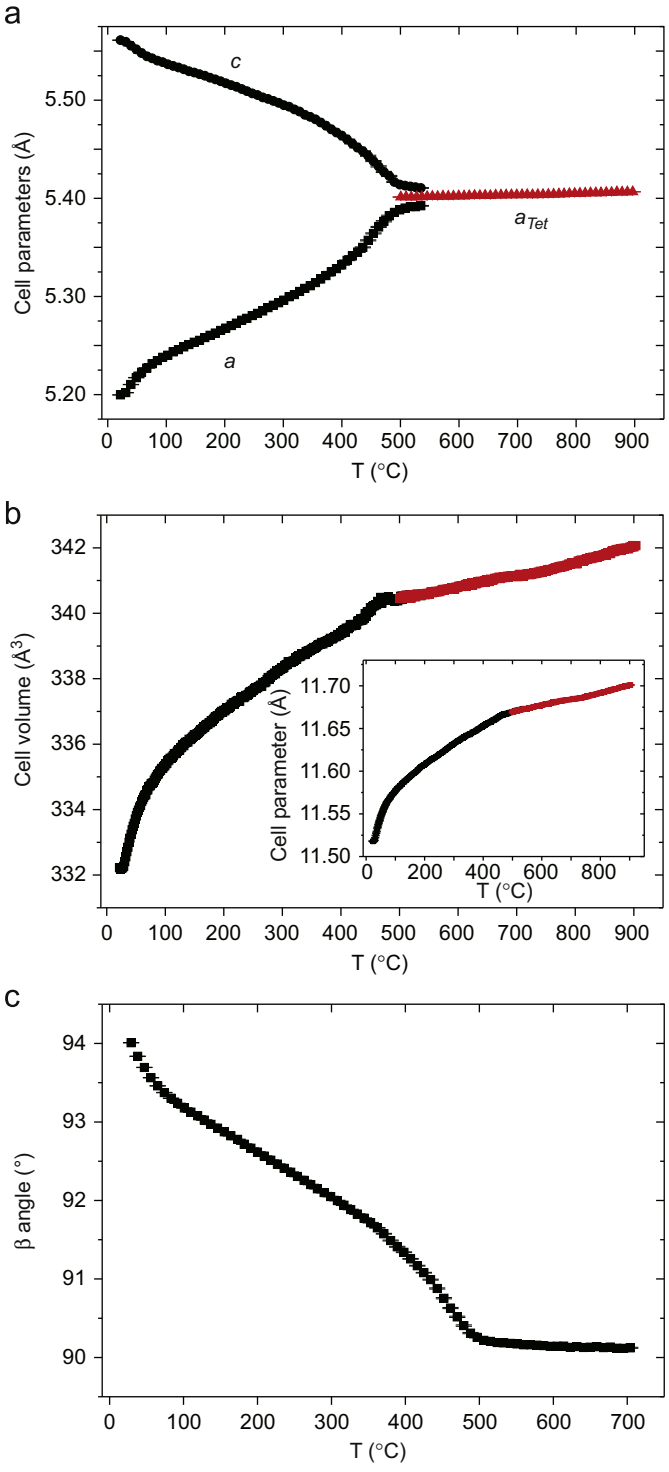

Fig. 5. Cell parameters for $LaNbO_4$ as a function of temperature derived from NPD ramping data. (a) Parameters a and c for the LT-monoclinic and a for the HT-tetragonal phase. (b) Cell volume with inset showing behavior of the long cell parameter (b for LT- and c for HT-phase). (c) β angle for the monoclinic phase. Error bars at one estimated standard deviation are included in the plots, but their magnitude is only clearly visible in c as they are significantly smaller than the symbols used.

capable of detecting microscopic elongations in all crystallographic directions. Microcracking, frequently observed in $LaNbO_4$ [10], is also a source of error in dilatometry measurements of polycrystalline ceramics, possibly contributing to the discrepancy of the TECs deduced from the two techniques.

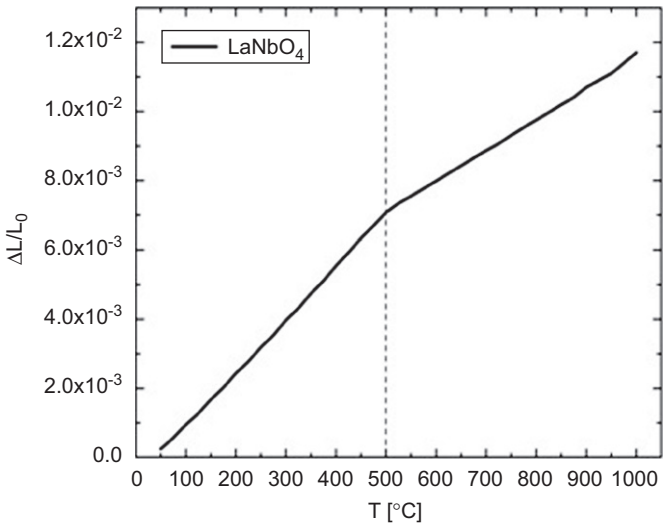

Fig. 6. Dilatometry (relative length change) from RT to 1000 °C for $LaNbO_4$ in wet Ar.

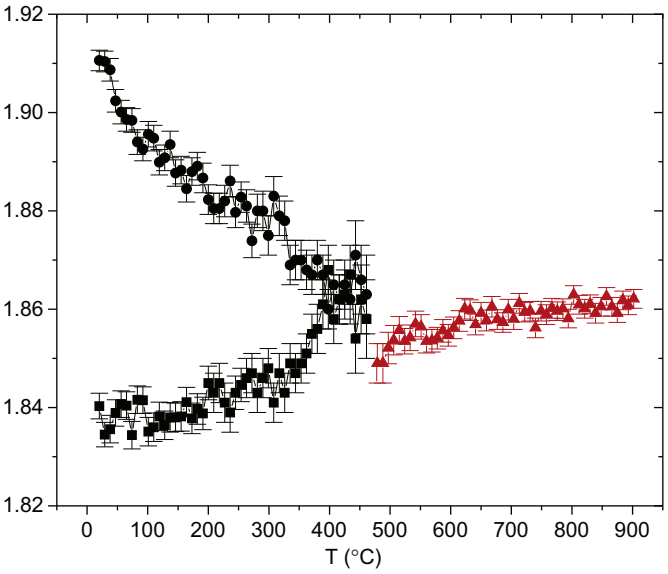

Fig. 7. Bond distances in the NbO_4 tetrahedra as a function of temperature. Circles represents Nb–O(1) and squares represents Nb–O(2) distances in m-$LaNbO_4$ whereas triangles denotes the Nb–O distance in t-$LaNbO_4$. Error bars at one estimated standard deviation are included in the plots.

Fig. 7 shows the temperature evolution of the bond distances within the NbO_4 tetrahedra. The behavior of the Nb–O(1) and Nb–O(2) bonds reflect the gradual change in the dimensions and geometry of the NbO_4-tetrahedra in the monoclinic phase with temperature. From Fig. 7 it can be seen that at RT the Nb–O(1) and Nb–O(2) distances are ~1.91 Å and 1.84 Å, respectively. Increasing the temperature results in a gradual decrease in the Nb–O(1) distance and a gradual increase of the Nb–O(2) distance until the transition temperature is reached. At this point the two oxygen sites become equivalent. On heating, the NbO_4-tetrahedra have undergone a gradual symmetry increase from highly distorted to a less-distorted geometry. The increasing bond length of Nb–O(1) with increasing temperature is comparable in magnitude to the bond length decrease of Nb–O(2), hence the resulting change in tetrahedra volume as a function of temperature is small (Vol. $NbO_{4(Mono.)}$=3.26 Å^3 and Vol. $NbO_{4(Tetrag.)}$=3.28 Å^3 from Tsunekawa [19] and David [4].

3.3. Proton migration in light of structure parameters

Based on density functional theory modeling (DFT) it has been suggested by Fjeld et al. [1] that an inter-tetrahedral proton mechanism is the rate limiting step in *m*-$LaNbO_4$. Fig. 8 shows the structure of *m*-$LaNbO_4$. The inset shows a magnified area where inter-tetrahedral proton migration is likely to occur, based on the stable proton sites and energy barriers reported by Fjeld et al. [1]. At RT there are two O(1) to O(1) distances of similar lengths (~2.97 Å), and the third closest O–O distance is ~3.09 Å and is between an O(1) and O(2) ion. These separations are labeled I, II and III, respectively in the Figure. The inter-tetrahedral proton transfer was suggested to be most likely to occur between a stable proton position approximately 1 Å from the O(1)-ion to an equivalent proton site near the O(1)-ion of the neighboring tetrahedra in the layer above, corresponding to pathway I in Fig. 8. As shown in Fig. 9a, this O(1)–O(1) distance decreases gradually with increasing temperature in the monoclinic polymorph, behavior that correlates well with the gradual change in enthalpy of proton mobility reported for *m*-$LaNbO_4$ [1]. In contrast it is difficult to correlate the weak variation of the oxygen separations of pathway II (Fig. 9b) with the significant temperature dependence of the proton mobility, and it therefore seems unlikely that it is an important proton migration path in *m*-$LaNbO_4$. It is, furthermore, doubtful that pathway III (O(1) to O(2)) contributes to the proton conductivity at low temperatures, despite its thermal contraction being similar to that of separation I (Fig. 9c). This is rationalized by the fact that the O(2) site is found to be significantly less energetically stable for protons compared to O(1) in *m*-$LaNbO_4$ and by the fact that the positively charged La-ion is located in close vicinity of this pathway and will repel the migrating protons [1].

In the tetragonal polymorph, separation I is basically temperature independent, a finding consistent with the constant enthalpy of proton mobility reported for *t*-$LaNbO_4$, hence this proton pathway is likely to be of importance also at high temperature. In the high temperature polymorph, separation III is also constant with temperature, and is approximately 0.14 Å longer than I. It may be tempting to suggest that this migration path also plays a role at high temperatures, but closer inspection of the structure reveals that the La-ion will repel the proton and hinder proton motion along this trajectory, in accordance with the analysis of *m*-$LaNbO_4$ [1].

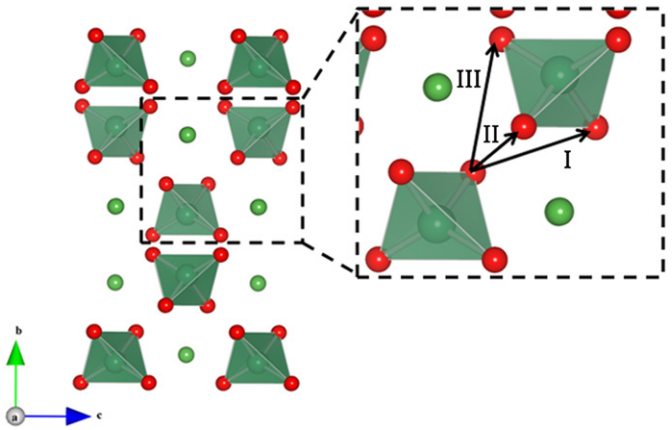

Fig. 8. Structure of monoclinic $LaNbO_4$, Oxygen (red spheres), lanthanum (green spheres) and niobium (inside tetrahedra). Inset: Magnified area where proton migration is likely to occur. Arrows indicate possible inter-tetrahedral proton migration distances: Pathway I – first O(1)–O(1) distance, II – second O(1)–O(1) distance, III – O(1)–O(2) separation. (For interpretation of the references to color in this figure legend, the reader is referred to the web version of this article.)

Proton transport in hydrated oxides is a complex compromise between primary and secondary (hydrogen) O–H bond formation and breaking, rigidity of the oxygen sub-lattice, and repulsing forces

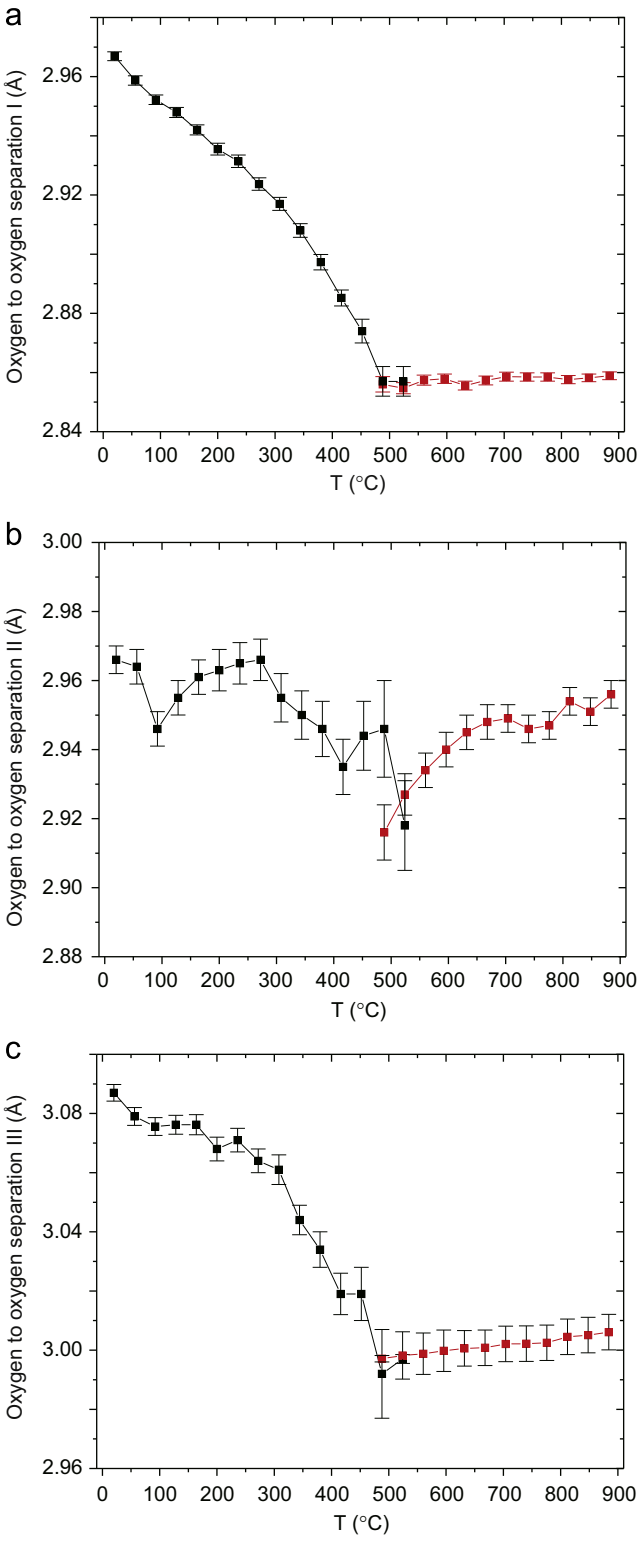

Fig. 9. Oxygen to oxygen separations as a function of temperature. Black points represent inter-atomic distances extracted using a monoclinic structural model, whereas red points were obtained using a tetragonal model; (a) inter-tetrahedral O(1)–O(1) distance I, (b) inter-tetrahedral O(1)–O(1) distance II, and inter-tetrahedral O(1)–O(2) distance. See Fig. 8 for definition of the distances I to III. Error bars at one estimated standard deviation are included in the plots. (For interpretation of the references to color in this figure legend, the reader is referred to the web version of this article.)

from surrounding cations (e.g. [24]). In recent modeling and experimental studies the proton conductivity of a similar material, $La_{1-x}Ba_{1+x}GaO_4$, has been studied in detail [25]. The structure of $La_{1-x}Ba_{1+x}GaO_4$ contains isolated GaO_4 units analogous to $LaNbO_4$, but in contrast to $LaNbO_4$ the modeling of $La_{1-x}Ba_{1+x}GaO_4$ reveals that the rate limiting step for proton transport is *intra*-tetrahedral proton transfer rather than inter-tetrahedral, i.e. the proton motion around a GaO_4 unit is of greatest importance. The arrangement of the distorted GaO_4 tetrahedra is such that it leads to activation energies for inter-tetrahedral motion that are small, and proton migration is predicted to be facilitated by short inter-tetrahedral O–O separations (<3 Å) leading to significant hydrogen-bonding [26]. Similar reasoning can be used to rationalize the decreasing enthalpy of proton mobility as the structural transition in $LaNbO_4$ is approached, i.e. as the key O–O distance (separation I) shrinks from 2.97 Å to 2.86 Å the strength of hydrogen-bonding is expected to increase enabling more facile inter-tetrahedral proton jumps. Consequently, we argue that the $\sim$4% contraction of this O(1) to O(1) distance is the primary structural factor that explains the decrease in enthalpy of proton mobility. This conclusion is further strengthened by the striking correlation shown in Fig. 10 that plots the temperature dependence of the enthalpy of proton migration (ΔH_{mob}) and the O(1) to O(1) separation denoted by pathway I. The activation energy plotted in the Figure was extracted from the Arrhenius plot of a sample of $La_{0.995}Sr_{0.005}NbO_{4-\delta}$ collected in a hydrated H_2/Ar mixture by first determining the pre-exponential term (σ_0) from the linear high T region (560–630 °C). The enthalpy of migration was then calculated as a function of temperature according to $\Delta H_{mob} = RT(\ln\sigma_0 - \ln\sigma_{bulk}T)$ as explained in further detail in [1].

To gain further insight into the proton environments in $LaNbO_4$ FT–IR spectra were collected on 0.5% Sr-doped $LaNbO_4$. Fig. 11 shows the infrared absorbance spectra over the O–H stretch region (2200–4500 cm^{-1}). Here, the larger intensity of the O–H stretch band for the hydrated sample confirms the presence of protons in this sample, whereas for the dehydrated sample the O–H stretch band-intensity is still clearly visible reflecting the difficulty to remove all protons from the structure although the sample has been annealed under vacuum at high temperatures.

For the hydrated sample, the O–H stretch band is between 2500 and 3700 cm^{-1}. The spread of energies observed in the IR spectra, in particular the low energy tail below $\sim$3300 cm^{-1} represent a significant shift from the O–H stretch of the free water molecule $\sim$3657 cm^{-1} [27], providing experimental evidence for moderate strength hydrogen bonded positions, possibly attributable to protons experiencing interactions with neighboring inter-tetrahedral O(1) ions. The spectra differ from that reported recently for protonated $La_{0.8}Ba_{1.2}GaO_{4-\delta}$ [26], in which significant absorption is seen in the region below 2500 cm^{-1}, and is taken to indicate a large proportion of protons that are strongly hydrogen bonded. Increased levels of strongly hydrogen bonded protons are also seen in very heavily doped $BaZr_{1-x}In_xO_{3-\delta}$ ($x \geq 0.5$) perovskites [28]. In both these systems the proton mobility is influenced by the balance between proton jumps, which are assisted by transient hydrogen-bonding, and re-orientation steps that involve breaking such bonds. For $LaNbO_4$ the proton migration pathway is also suggested to involve both rotation and transfer steps in order to achieve long range "in-plane" diffusion [1]. The ideal strength of hydrogen bonding for fast proton transport in these systems remains to be clarified. It is likely to vary from material to material reflecting the local structure and particular rate determining steps.

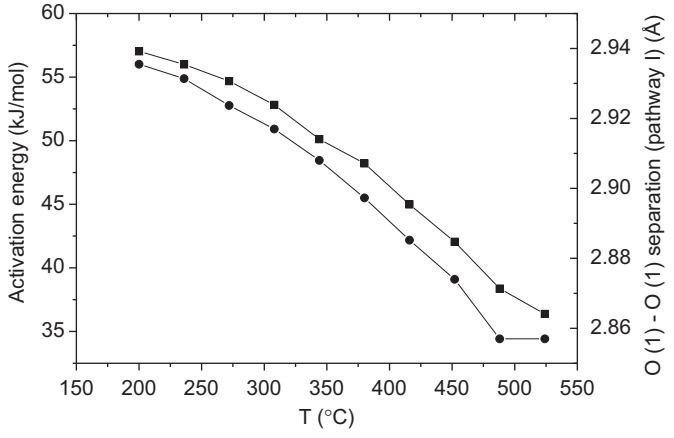

Fig. 10. Temperature dependence of the enthalpy of proton motion (squares) and O(1)–O(1) separation (pathway I, Fig. 8) circles.

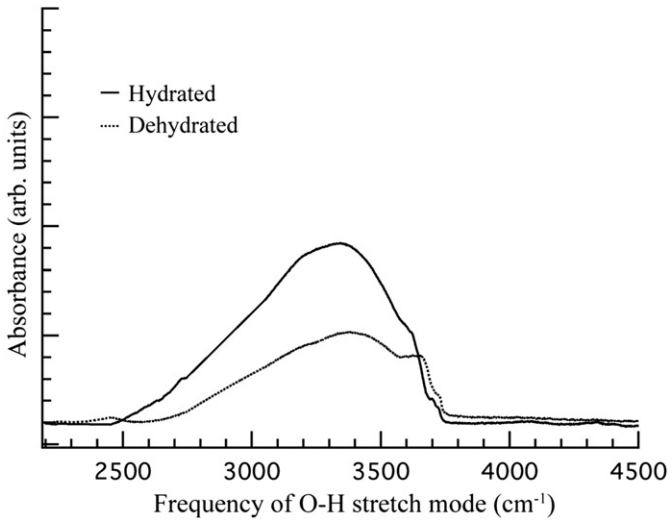

Fig. 11. Infrared spectra of $La_{0.995}Sr_{0.005}NbO_{4-\delta}$.

4. Conclusions

The crystal structure of $LaNbO_4$ has been characterized by high intensity variable temperature neutron powder diffraction. Special emphasis was placed on the structural changes through the second order phase transition from the monoclinic to the tetragonal polymorph with increasing temperature. The negative thermal expansion of the O(1) to O(1) inter-tetrahedral distance (pathway I) means that it emerges as the most probable rate limiting proton transport trajectory in monoclinic $LaNbO_4$. In tetragonal $LaNbO_4$, the same oxygen–oxygen inter-tetrahedral distance was found to be more or less constant with temperature, again in line with the reported unvarying enthalpy of proton mobility. The present analysis successfully links the thermal evolution of a key structural parameter with previous computational studies and experimental measurements of proton mobility in acceptor-doped $LaNbO_4$ to explain the impact of the evolving crystal structure on the proton conductivity.

Acknowledgments

This work has been funded by The Research Council of Norway (project nr. 187160/S30) under The Northern European Innovative Energy Research Program (N-INNER) in the project entitled "Novel High-Temperature Proton and Mixed-Proton Electron Conductors for Fuel Cells and H_2-Separation Membranes". CSK and MK are also grateful to the Swedish Research Council (Vetenskapsrådet) for funding. The Institut Laue Langevin is

thanked for neutron beam time allocation and Paul Henry is thanked for assisting the D20 experiments. Harald Fjeld, University of Oslo is also thanked for useful discussions.

References

[1] H. Fjeld, K. Toyoura, R. Haugsrud, T. Norby, PCCP 12 (2010) 10313.
[2] T. Esaka, Solid State Ionics 136–137 (2000) 1.
[3] R. Haugsrud, T. Norby, Nat. Mater. 5 (2006) 193.
[4] W.I.F. David, Mater. Res. Bull. 18 (6) (1983) 749.
[5] L. Jian, M. Wayman, J. Am. Ceram. Soc. 80 (3) (1997) 803.
[6] R.B. Ferguson, Can. Mineral. 6 (1957) 23.
[7] R. Haugsrud, T. Norby, Solid State Ionics 177 (2006) 1129.
[8] L.Y. Wang, C. Kjølseth, R. Haugsrud, T. Norby, Personal Communication.
[9] D. Errandonea, Europhys. Lett. 77 (2007) 56001.
[10] T. Mokkelbost, I. Kaus, R. Haugsrud, T. Norby, T. Grande, M.-A. Einarsrud, J. Am. Ceram. Soc. 91 (3) (2008) 879.
[11] T. Mokkelbost, H.L. Lein, P.E. Vullum, R. Holmestad, M.-A. Einarsrud, T. Grande, Ceram. Int. 35 (2009) 2877.
[12] L. Jian, M. Wayman, J. Am. Ceram. Soc. 79 (1996) (1642) 6.
[13] M. Machida, J. Kido, T. Kobayashi, S. Fukui, N. Koyano, Y. Suemune, Kyoto University, Research Reactor Institute: Annual Report 28 (1995) 25.
[14] G.C. Mather, C.A.J. Fisher, M.S. Islam, Chem. Mater. 22 (2010) 5912.
[15] A. Neumann, D. Walter, Thermochim. Acta 445 (2006) 200.
[16] J. Rodriguez-Carvajal, Physica B 192 (1993) 55.
[17] T.C. Hansen, P.F. Henry, H.E. Fisher, J. Torregrossa, P. Convert, Meas. Sci. Technol. 19 (2008) 034001.
[18] A.C. Larson, R.B. Von Dreele, Los Alamos National Laboratory Report LAUR 86-748 (1994).
[19] S. Tsunekawa, T. Kamiyama, K. Sasaki, H. Asano, T. Fukuda, Acta Crystallogr., Sect. A 49 (1993) 595.
[20] V.S. Stubican, J. Am. Ceram. Soc. 47 (1964) 55.
[21] L. Malavasi, C. Ritter, G. Chiodelli, J. Alloys Compd. 475 (2008) L42.
[22] F. Vullum, F. Nitsche, S.M. Selbach, T. Grande, J. Solid State Chem. 181 (2008) 2580.
[23] O. Prytz, J. Taftø, Acta Mater. 53 (2004) 297.
[24] K.D. Kreuer, Annu. Rev. Mater. Res. 33 (2003) 333.
[25] E. Kendrick, J. Kendrick, K.S. Knight, S.M. Islam, P. Slater, Nat. Mater. 6 (2007) 871.
[26] F. Giannici, D. Messana, A. Longo, A. Martorana, J. Phys. Chem. C 115 (2011) 298.
[27] A. Lock, H. Bakker, J. Chem. Phys. 117 (2002) 1708.
[28] M. Karlsson, M.E. Björketun, P.G. Sundell, A. Matic, G. Wahnström, D. Engberg, L. Börjesson, P. Berastegui, Phys. Rev. B 72 (2005) 094303.